Research Article
Molecular and Cell Biology

JOURNAL
OF HEPATOLOGY

The long non-coding RNA *LncHDAC2* drives the self-renewal of liver cancer stem cells via activation of Hedgehog signaling

Graphical abstract

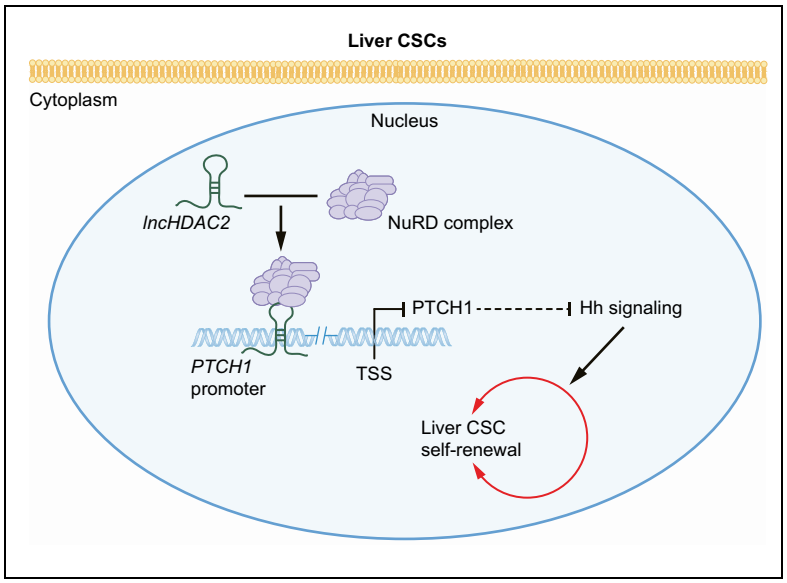

Highlights

- Long non-coding RNA *lncHDAC2* is highly expressed in liver cancer stem cells.
- *LncHDAC2* promotes the self-renewal of liver cancer stem cells.
- *LncHDAC2* associates with HDAC2 in liver cancer stem cells.
- *LncHDAC2*-mediated PTCH1 downregulation promotes Hh signaling, driving self-renewal of liver cancer stem cells.

Authors

Jiayi Wu, Pingping Zhu, Tiankun Lu, ..., Yajing Hao, Lei He, Zusen Fan

Correspondence

fanz@moon.ibp.ac.cn
(Z. Fan)

Lay summary

Liver cancer stem cells harbor high tumor-initiating potential and confer resistance to typical therapies, but the mechanism underlying their self-renewal remains elusive. *LncHDAC2* augments the self-renewal of these cells, promoting tumor propagation. In liver cancer stem cells, *lncHDAC2* activates Hedgehog signaling to initiate liver tumorigenesis. Therefore, *lncHDAC2* and the Hedgehog signaling pathway may serve as biomarkers and potential drug targets for hepatocellular carcinoma.

http://dx.doi.org/10.1016/j.jhep.2018.12.015
 J. Hepatol. 2019, 70, 918–929

Research Article
Molecular and Cell Biology

JOURNAL OF HEPATOLOGY

The long non-coding RNA *LncHDAC2* drives the self-renewal of liver cancer stem cells via activation of Hedgehog signaling

Jiayi Wu[1,2,†], Pingping Zhu[1,†], Tiankun Lu[1,2,†], Ying Du[1,†], Yanying Wang[1,†], Luyun He[1,2], Buqing Ye[1], Benyu Liu[1], Liuliu Yang[1,2], Jing Wang[1,2], Yang Gu[1,2], Jie Lan[2,3], Yajing Hao[2,3], Lei He[4], Zusen Fan[1,2,*]

[1]*CAS Key Laboratory of Infection and Immunity, CAS Center for Excellence in Biomacromolecules, Institute of Biophysics, Chinese Academy of Sciences, Beijing 100101, China;* [2]*University of Chinese Academy of Sciences, Beijing 100049, China;* [3]*Key Laboratory of RNA Biology, Institute of Biophysics, Chinese Academy of Sciences, Beijing 100101, China;* [4]*Department of Hepatobiliary Surgery, PLA General Hospital, Beijing 100853, China*

Background & Aims: Liver cancer is the second leading cause of cancer death worldwide. Hepatocellular carcinoma (HCC) is the most common type of primary liver cancer in adults. The aim of this study was to define the role of the long non-coding RNA *lncHDAC2* in the tumorigenesis of HCC.

Methods: $CD13^{+}CD133^{+}$ cells (hereafter called liver cancer stem cells [CSCs]) and $CD13^{-}CD133^{-}$ cells (referred to as non-CSCs) were sorted from 3 primary HCC tumor tissues and followed by transcriptome microarray. The expression and function of *lncHDAC2* were further assessed by northern blot, sphere formation and xenograft tumor models.

Results: *LncHDAC2* is highly expressed in HCC tumors and liver CSCs. *LncHDAC2* promotes the self-renewal of liver CSCs and tumor propagation. In liver CSCs, *lncHDAC2* recruits the NuRD complex onto the promoter of *PTCH1* to inhibit its expression, leading to activation of Hedgehog signaling. Moreover, HDAC2 expression levels are positively related to HCC severity and PTCH1 levels are negatively related to HCC severity. Additionally, the Smo inhibitor cyclopamine was shown to impair the self-renewal of liver CSCs and suppress tumor propagation.

Conclusion: Our findings reveal that *lncHDAC2* promotes the self-renewal of liver CSCs and tumor propagation by activating the Hedgehog signaling pathway. Downregulating lncHDAC2 is a promising antitumor strategy in HCC.

Lay summary: Liver cancer stem cells harbor high tumor-initiating potential and confer resistance to typical therapies, but the mechanism underlying their self-renewal remains elusive. *LncHDAC2* augments the self-renewal of these cells, promoting tumor propagation. In liver cancer stem cells, *lncHDAC2* activates Hedgehog signaling to initiate liver tumorigenesis. Therefore, *lncHDAC2* and the Hedgehog signaling pathway may serve as biomarkers and potential drug targets for hepatocellular carcinoma.

Keywords: Hepatocellular carcinoma; Cancer stem cell; lncHDAC2; HDAC2; PTCH1.
Received 27 August 2018; received in revised form 20 November 2018; accepted 7 December 2018; available online 22 December 2018

* Corresponding author. Address: The CAS key Laboratory of Infection and Immunity, Institute of Biophysics, Chinese Academy of Sciences, Beijing 100101, China. Tel.: +86 10 64888457, fax: +86 10 64871293.
E-mail address: fanz@moon.ibp.ac.cn (Z. Fan).
† These three authors contributed equally to this paper.

Introduction

Hepatocellular carcinoma (HCC), the most common type of primary liver cancer, is one of the leading causes of cancer death globally. The highest incidence of HCC is in East and South-East Asia and Northern and Western Africa.[1] However, the incidence of liver cancer, including HCC, has risen in areas with historically low rates, for instance, Western Europe, Northern America and parts of Oceania. Infection with hepatitis B virus and hepatitis C virus, as well as metabolic disorders, are etiologically responsible for HCC.[2] The high rate of recurrence and heterogeneity render HCC intractable.[3] Therefore, the mechanism underlying liver carcinogenesis remain elusive.

Most human tumors exhibit cellular heterogeneity due to inherently high genetic instability, resulting in the evolution of cells with the capacity of tumor initiation. Cancer stem cells (CSCs) refer to a subset of tumor cells with many phenotypic and functional properties of normal stem cells, including the ability of self-renewal and differentiation.[4–6] Numerous cell surface markers have been identified to isolate liver CSCs, including CD13, CD133, EpCAM, CD24, CD90 and CD44.[7,8] CSCs display some characteristics of embryonic or tissue stem cells, and typically harbor persistent activation of one or more highly conserved stemness signaling pathways, such as Hedgehog (Hh), Notch, and Wnt pathways.[9–11] Activation of the Hh signaling pathway is implicated in the initiation of distinct cancers of the liver, brain, muscle and skin.[12–15] The Hh ligands include Sonic (Shh), Desert (Dhh) and Indian (Ihh) Hh, which initiate a signaling cascade via binding with their common receptor Patched 1 (PTCH1).[16] Following Hh engagement, PTCH1 stops inhibiting the regulatory transmembrane protein Smoothened (Smo), allowing it to migrate to the tip of the primary cilium and activate Gli transcription factors that drive tumor initiation.[17] However, how Hh signaling regulates liver CSCs remains largely unknown.

Over the past 2 decades, overwhelming evidence has demonstrated the regulatory roles of different classes of non-coding RNAs (ncRNAs) in liver carcinogenesis.[18,19] Among these ncRNAs, transcripts longer than 200 nucleotides are termed long non-coding RNAs (lncRNAs). LncRNAs are involved in a wide range of biological processes.[20–22] We recently defined several lncRNAs that promote the self-renewal of human liver cancer stem cells.[23–25] In this study, we identified another highly expressed lncRNA in primary liver CSCs that we called

lncHDAC2 (lncRNA for association with HDAC2, gene symbol ENST00000601096). LncHDAC2 associates with HDAC2 to suppress PTCH1 expression, which activates Hh signaling and sustains the stemness of liver CSCs.

Materials and methods

Antibodies and reagents

Phycoerythrin (PE)-conjugated CD133 (cat. no. 130098826) antibody was obtained from MiltenyiBiotec. Fluorescein isothiocyanate (FITC)-conjugated CD13 antibody (cat. no. 11-0138) was purchased from eBioscience. Anti-HDAC2 (cat. no. 5113P) antibody was purchased from Cell Signaling Technology. Anti-PTCH1 (cat. no. LS-C114391) antibody was from LifeSpan BioSciences. Anti-HDAC1 (cat. no. ab53091), anti-CHD3 (cat. no. ab85428) and anti-LSD1 (cat. no. ab17721) antibodies were obtained from Abcam. Anti-c-Myc (cat. no. sc-70469) and anti-GLI2 (cat. no. sc-271786) antibodies were from Santa Cruz. Alexa-594 and Alexa-488-conjugated secondary antibodies and horseradish peroxidase (HRP)-conjugated secondary antibodies were purchased from Invitrogen. N2 supplement and B27 supplement were from Invitrogen. bFGF (cat. no. GF446-50UG) was from Millipore. Anti-β-actin antibody (cat. no. A1978), DAPI (cat. no. 28718-90-3), EGF (cat. no. E5036-200UG) and PEG 5000 (cat. no. 175233-46-2) were from Sigma-Aldrich. The Chemiluminescent Nucleic Acid Detection Module (cat. no. 89880) and LightShift™ Chemiluminescent RNA EMSA kit (cat. no. 20158) were purchased from Thermo Scientific. Ultra-low attachment plates (cat. no. 3471) were from Corning Company.

Cell lines

HCC cell lines PLC/PRF/5 (PLC), Huh7 and HepG2 were from Dr. Zeguang Han (Shanghai Jiaotong University School of Medicine, Shanghai, China). HCC cells were maintained in DMEM medium supplemented with 10% fetal bovine serum, 100 μg/ml penicillin and 100 U/ml streptomycin. For preparation of HCC primary cells, HCC samples were immediately obtained after resection. Tumor bulk was cut into 1 mm^3 with scissors, followed by digestion with collagenase IV for 40 min (0.05% collagenase IV, 0.05% proteinase, 0.01% DNase and 5 mM $CaCl_2$ in HBS), with shaking every 10 min. Then the samples were passed through a 70 mm cell strainer and centrifuged at 50 g for 1 min. Supernatant fractions were collected and further centrifuged at 150 g for 8 min and HCC cells were enriched in pellets. After red cell elimination, HCC primary cells were obtained and used for other experiments.

Mice

Six-week-old female BALB/c nude mice were purchased from Beijing Vital River Laboratory Animal Technology Co. Ltd. Mice were housed 4 per cage in individually ventilated cage systems in specific-pathogen-free grade animal room and fed standard laboratory diet with water and food. Mouse were kept under a 12 h/12 h light/dark cycles. All experiments involving mice were approved by the institutional committee of Institute of Biophysics, Chinese Academy of Sciences.

LncHDAC2 knockdown

Antisense oligonucleotides (ASOs) against *lncHDAC2* were custom-designed using Exiqon's Antisense LNA GapmeR designer and a non-targeting ASO was included as a control. ASOs were resuspended in water to a final concentration of 100 mM. Primary HCC cells were nucleofected with 100 pmol of ASO. Changes in *lncHDAC2* expression were determined by quantitative PCR.

CRISPR/Cas9 knockout system

HDAC2 knockout (KO) and *PTCH1* KO cells were established via CRISPR/Cas9 approaches according to standard protocol provided by Zhang's lab. sgRNAs were generated by online CRISPR Design Tool (http://tools.genome-engineering.org) and cloned into LentiCRISPRv2 (puro, catalog 52961) vector. We generated lentivirus in 293 T cells and infected cells, followed by puromycin selection. To generate *lncHDAC2* KO and *PTCH1* promoter KO cells, we also used modified lentiCRISPRv2(GFP). A pair of sgRNAs from the left and right locus of the target region were cloned into puro lentiCRISPRv2 and GFP lentiCRISPRv2. Cells were infected and treated with puromycin and GFP double selection.

RNA EMSA assay

EMSA experiments were performed using a LightShift Chemiluminescent RNA EMSA Kit (Thermo Scientific).

RNA antisense purification and mass spectrometry

For probe screening, imbricate DNA probes against *lncHDAC2* transcript were designed, and incubated with nuclear fractions separated from oncospheres, followed by RNase H digestion for 1 h. Samples were analyzed for *lncHDAC2* integrity using northern blot (data not shown). Probes were grouped into Probeset-*LncHDAC2* when *lncHDAC2* was digested and grouped into Probeset-Ctrl when there was no influence on *lncHDAC2* integrity. Probes were then labeled with digoxin and incubated with nuclear fractions separated from oncospheres. After capture with digoxin antibody and protein A/G beads, RNase A and DNase were added to clean out nucleic acid. Enriched proteins were analyzed by SDS-PAGE gels, followed by mass spectrometry.

RNA immunoprecipitation (RIP)

Oncospheres were collected and treated with 1% formaldehyde for 15 min, then dissolved with RNase free RIPA buffer (150 mM NaCl, 0.5% sodium deoxycholate, 0.1% SDS, 1% NP40, 1 mM EDTA, 50 mMTris [pH 8.0]), supplemented with cocktail protease inhibitors and RNase inhibitor (Roche). The samples were sonicated on ice 3 times, followed by centrifugation at 12,000*g* for 10 min. Supernatants were then collected and incubated with protein A/G beads for pre-clear, followed by antibody incubation overnight, then protein A/G beads were added. Total RNA was extracted from the eluent, and *LncHDAC2* enrichment was examined by quantitative PCR.

Northern blot

Total RNA was extracted from HCC samples or oncospheres using standard TRZIOL methods, followed by electrophoresis with formaldehyde denaturing agarose gel. Samples were transferred to positively charged NC film (Beyotime Biotechnology) using 20× SSC buffer (3.0 M NaCl, 0.3 M sodium citrate, pH7.0). After UV cross-linking, membrane was incubated with hybrid buffer for 2 h prehybridization, followed by incubation with biotin labeled RNA probes generated by *in vitro* transcription at 65 °C for 20 h. Biotin signals were detected with HRP-conjugated streptavidin according to the introduction of Chemiluminescent Nucleic Acid Detection Module (Thermo Scientific).

For northern blot, the biotin labeled RNA probe matching the exon-exon junction was used.

Chromatin isolation by RNA purification-PCR assay
Chromatin isolation by RNA purification (ChIRP) assay was performed according to the standard procedure. Briefly, oncospheres were cross-linked with 1% glutaraldehyde, followed by lysis buffer treatment and subsequent sonication. Two sets of digoxin labeled *LncHDAC2* probes (Probeset-*LncHDAC2* and Probeset-Ctrl) were added into samples for incubation at 37 °C for 4 h with shaking. Combined chromatin fragments were enriched by digoxin antibody and protein A/G before being purified for quantitative PCR examination.

Chromatin immunoprecipitation
Chromatin immunoprecipitation (ChIP) was performed according to the standard protocol (Upstate Biotechnology, Inc.). In brief, oncospheres were fixed in 1% formaldehyde for 10 min at 37 °C, and then cracked by SDS lysis buffer for 10 min on ice, followed by sonication to shear DNA into fragments between 200 and 500 base pairs. Anti-HDAC2 antibody was used for the ChIP assay as described.

Sphere-formation assay
One thousand PLC or Huh7 cells were grown in sphere-formation medium (DMEM supplemented with 20 ng/ml bFGF, 20 ng/ml EGF, N2 and B27). Two weeks later, spheres larger than 100 μm were counted and photographs were taken. For HCC samples, 5,000 primary cells were used for sphere formation. The spheres were fixed for immunofluorescence staining or digested for co-immunoprecipitation and western blot assays. For non-sphere cell separation, we collected sphere-formation medium that contains non-sphere cells and sphere cells in an Eppendorf tube and let this stand for 5 min, at this stage the pellets contained sphere cells. Supernatants were then moved into a new Eppendorf tube carefully with transferpettor and collected by centrifugation at 1,500*g* for 5 min. Pellets now contained non-sphere cells which were used directly for subsequent experiments. We cultured these non-sphere cells under the same non-adherent conditions as sphere cells.

Flow cytometry
Cells were labeled with FITC-conjugated CD13 and PE-conjugated CD133 antibodies followed by CSC isolation. For FACS analysis, cells were incubated with fluorescence-conjugated antibodies or with primary antibodies and further fluorescence-conjugated secondary antibodies.

Xenograft growth in nude mice
For subcutaneous injection models, gradient dilutions of control and treated cells were implanted into mice (male BALB/c nude mice), aged 6 weeks, with a matrigel scaffold (BD matrigel matrix, BD biosciences) into 2 sides of the same nude mice at the posterior dorsal flank region (n = 6 to 12 per group). Tumors were measured every 4 days.

Diluted xenograft tumor formation
BALB/c nude mice were injected with 10, 1×10^2, 1×10^3, 1×10^4 and 1×10^5 cells. Three months later, tumor formation was counted, followed by calculation of ratios of tumor-free mice and tumor-initiating cells.

Luciferase reporter assay
Luciferase reporter assay was performed according to the standard protocol of Dual-Luciferase Reporter Assay system (Promega). Briefly, indicated fragments of *PTCH1* promoter were cloned into the pGL3 luciferase reporter vector and transfected into HDAC2 or *lncHDAC2* overexpression and control Huh7 cells. For each sample, 1 ng pRL-TK was transfected as loading control. Cells were collected and lysed by lysis buffer 36 h later, after which luciferase activity was determined.

Immunohistochemistry assay
Formalin-fixed tumor tissue sections were deparaffinized in xylene (10 min, twice), rehydrated in graded alcohols (100%, 100%, 95%, 85%, and 70% alcohols), and finally submerged in distilled water. After treated in 3% hydrogen peroxide (H_2O_2) for 15 min, the slides were processed for antigen retrieval in Tris-EDTA buffer (10 mM, pH 8.0), 121 °C for 5 min, and then cooled down slowly. After blocking with 10% goat serum for 30 min, the sections were incubated in primary antibodies overnight. After washing 3 times with PBS, the sections were incubated in HRP-conjugated secondary antibodies, and subsequent detection was performed using the standard substrate detection of HRP. Then, the sections were stained with hematoxylin and dehydration in graded alcohols and xylene.

Immunofluorescence staining
Cells were fixed by 4% paraformaldehyde (PFA) for 20 min and penetrated by 0.5% tritonX-100 for 30 min. After blocking with 10% fetal bovine serum, primary antibodies were added and incubated overnight at 4 °C. After washing 3 times with PBS, fluorescence-conjugated secondary antibodies were added for observation by confocal microscopy.

Study approval
All HCC specimens were obtained from the partial hepatectomy series at the Department of Hepatobiliary Surgery, PLA General Hospital (Beijing, China) with informed consents, according to the Institutional Review Board approval. We numbered HCC primary samples according to the date received and utilized the samples without artificial bias.

HTA 2.0 transcriptome microarray assay
Total RNA was isolated with Trizol from $CD133^+CD13^+$ cells and $CD133^-CD13^-$ cells derived from HCC primary samples. Biotinylated cDNA was prepared according to the standard Affymetrix protocol from 250 ng total RNA by using Ambion® WT Expression Kit. Following labeling, 5.5 μg of cDNA was hybridized for 16 h at 45 °C on GeneChip Human Transcriptome Array 2.0. GeneChips were washed and stained in the Affymetrix Fluidics Station 450. GeneChips were scanned by using Affymetrix® GeneChip Command Console (AGCC) that installed in GeneChip® Scanner 3000 7 G. Data were analyzed with Robust Multichip Analysis (RMA) algorithm using Affymetrix default analysis settings. Values presented are log2 RMA signal intensity. Microarray data have been deposited in the NCBI GEO under accession number GSE122420.

Statistical analysis
For statistical evaluation, an unpaired Student's *t* test was applied for calculating statistical probabilities in this study. For survival analysis, the Kaplan-Meier survival analysis was used. Statistical calculation was performed using Excel 2010.

p <0.05 was considered significant ($^{*}p$ <0.05; $^{**}p$ <0.01; $^{***}p$ <0.001); p > 0.05, non-significant. All flow cytometry data were analyzed with FlowJo (Treestar).

For further details regarding the materials used, please refer to the CTAT table.

Results

LncHDAC2 is highly expressed in liver CSCs

We previously identified several lncRNAs from liver CSCs of HCC cell lines and defined their roles in the modulation of liver CSC stemness.[23–25] To further identify physiological lncRNAs involved in liver CSCs, we conducted transcriptome microarray analysis of $CD13^{+}CD133^{+}$ cells (hereafter called liver CSCs) and $CD13^{-}CD133^{-}$ cells (referred to as non-CSCs) sorted from 3 HCC primary tumor tissues (Fig. S1A). Indeed, $CD13^{+}CD133^{+}$ cells harbored stemness capacity through oncosphere formation, stemness analysis and tumor formation in xenograft models (Fig. S1B–D). Through analysis of these transcriptome profiles, 665 upregulated and 412 downregulated lncRNAs were identified (Fig. 1A). Among the top 20 upregulated intergenic lncRNAs in liver CSCs, we focused on the *lncHDAC2* (gene symbol: ENST00000601096), whose depletion most significantly suppressed oncosphere formation (Fig. 1B). *LncHDAC2*, located on chromosome 9 in humans, containing 2 exons and comprised 834 nucleotides (Fig. 1C), whose full-length was further amplified by RACE (rapid-amplification of cDNA ends) and validated by sequencing (Fig. S2A). In addition, *lncHDAC2* showed no protein coding potentiality (Fig. S2B, C). *LncHDAC2* was expressed in HCC primary tumor tissues through *in situ* hybridization (Fig. 1D) and further validated by Northern blot (Fig. 1E).

Owing to high expression levels of *lncHDAC2* in liver CSCs based on transcriptome data, we next verified *lncHDAC2* expression in liver CSCs from HCC primary samples. We found that *lncHDAC2* was indeed highly expressed in liver CSCs derived from HCC primary samples (Fig. S2D). We noticed that *lncHDAC2* was also highly expressed in oncosphere cells derived from HCC primary samples and HCC cell lines (Fig. 1F, G and Fig. S2E, F). In addition, *lncHDAC2* mainly located in the nuclei of HCC cells by RNA fluorescence *in situ* hybridization (RNA-FISH) (Fig. 1F). These observations were further validated by nuclear and cytoplasmic fractionation of liver CSCs (Fig. 1H and Fig. S2G). Altogether, *lncHDAC2* is expressed in HCC tumor tissues and highly expressed in liver CSCs.

LncHDAC2 promotes the self-renewal of liver CSCs

We next wanted to explore the role of *lncHDAC2* in the self-renewal of liver CSCs. We depleted *lncHDAC2* in 6 HCC primary tumor cells by ASOs (Fig. 2A and Fig. S3A), followed by sphere-formation assays. We observed that *lncHDAC2* depletion markedly inhibited sphere formation (Fig. 2A). Reduced self-renewal capacity was further validated in *lncHDAC2* silenced cells through serial sphere-formation assays (Fig. 2B). We also established *lncHDAC2* KO cells (Fig. S3B) and injected 1×10^{6} *lncHDAC2* KO and sgCtrl cells into BALB/c nude mice, followed by measurement of tumor volumes every 4 days. *LncHDAC2* KO cells significantly reduced tumor propagation compared to sgCtrl treated cells (Fig. 2C). Furthermore, *lncHDAC2* KO displayed much weaker tumor initiation and tumorigenic cell frequency as assayed by a limiting dilution xenograft analysis (Fig. 2D). These data suggest that *lncHDAC2* deletion impairs the stemness of liver CSCs.

We then established *lncHDAC2* stably overexpressing HCC primary cells via lentivirus and examined oncosphere formation and self-renewal capacities. We found that *lncHDAC2* overexpression promoted *in vitro* oncosphere formation (Fig. 2E, F), as well as augmented *in vivo* tumor propagation and tumorigenic cell frequency (Fig. 2G, H). Taken together, *lncHDAC2* promotes the self-renewal of liver CSCs and *in vivo* tumor propagation.

LncHDAC2 associates with HDAC2 in liver CSCs

LncRNAs are considered to exert their regulatory functions in *trans* or in *cis*.[26–28] Of note, we observed that *lncHDAC2* depletion did not impact the expression of its nearby genes (Fig. S4A), suggesting that *lncHDAC2* exerts its function in *trans*. RNA antisense purification has been used as a critical strategy to identify RNA-binding proteins.[29] We then screened probes against *lncHDAC2* transcript with RNase H treatment and labeled them with digoxin. These labeled probes were incubated with oncosphere cell lysates and analyzed by silver staining (Fig. 3A). With mass spectrometry, the differential band binding to *lncHDAC2* was identified to be HDAC2, a major component of the NuRD remodeling complex.[30,31] The interaction of *lncHDAC2* with HDAC2 was further confirmed by western blot (Fig. 3B) and RNA immunoprecipitation assay (Fig. 3C). The co-localization of *lncHDAC2* with HDAC2 in oncosphere cells derived from HCC primary cells was validated by immunofluorescence staining and mainly distributed in the nucleus (Fig. 3D). A stable stem-loop structure at the *lncHDAC2* exon1 was predicted by RNA folding analysis (Fig. S4B). Through domain mapping, we identified that region of *lncHDAC2* exon1 (nucleotide 1–364) was necessary and sufficient to bind HDAC2 (Fig. 3E). *LncHDAC2* depletion impaired the self-renewal and tumor propagation capacity of HCC primary cells (Fig. 2A, C). However, overexpression of mutant *lncHDAC2* without the HDAC2 binding domain in *lncHDAC2* depleted cells failed to rescue the phenotype (Fig. 3F, G). Altogether, *lncHDAC2* interacts with HDAC2 in liver CSCs.

LncHDAC2 recruits the NuRD complex onto the promoter of *PTCH1* gene to suppress its expression

We next detected expression levels of main self-renewal-related pathways in *lncHDAC2* KO oncosphere cells. We found that *lncHDAC2* deletion dramatically suppressed Hh signaling (Fig. 4A). Through ChIRP assay, we found that *lncHDAC2* was enriched on the 1,200–1,400 bp region of the *PTCH1* promoter, upstream of the transcriptional start site (Fig. 4B). By contrast, *lncHDAC2* did not bind to other gene promoters of Hh signaling target genes (Fig. S5). We thus focused on the *PTCH1* gene in the regulation of Hh signaling mediated by *lncHDAC2* in liver CSCs. In addition, HDAC2 also bound to the same region of *PTCH1* promoter as *lncHDAC2* did via ChIP assay (Fig. 4C). Of note, the interaction of *lncHDAC2* and HDAC2 with the *PTCH1* promoter was validated by the EMSA assay (Fig. 4D). With cross-linking treatment, *lncHDAC2* was co-eluted with the NuRD complex in oncosphere lysates via ChIP and ChIRP assays (Fig. 4E, F). We also noticed that *lncHDAC2* or HDAC2 deletion significantly facilitated *PTCH1* promoter activation by DNase I sensitivity assays (Fig. 4G). To confirm that PTCH1 was suppressed by *lncHDAC2* and HDAC2, we performed luciferase reporter assays. We observed that *lncHDAC2* and HDAC2 bound to *PTCH1* promoter, whereas the mutant *lncHDAC2* without HDAC2 binding domain did not (Fig. 4H). In parallel, anti-HDAC2 antibody did

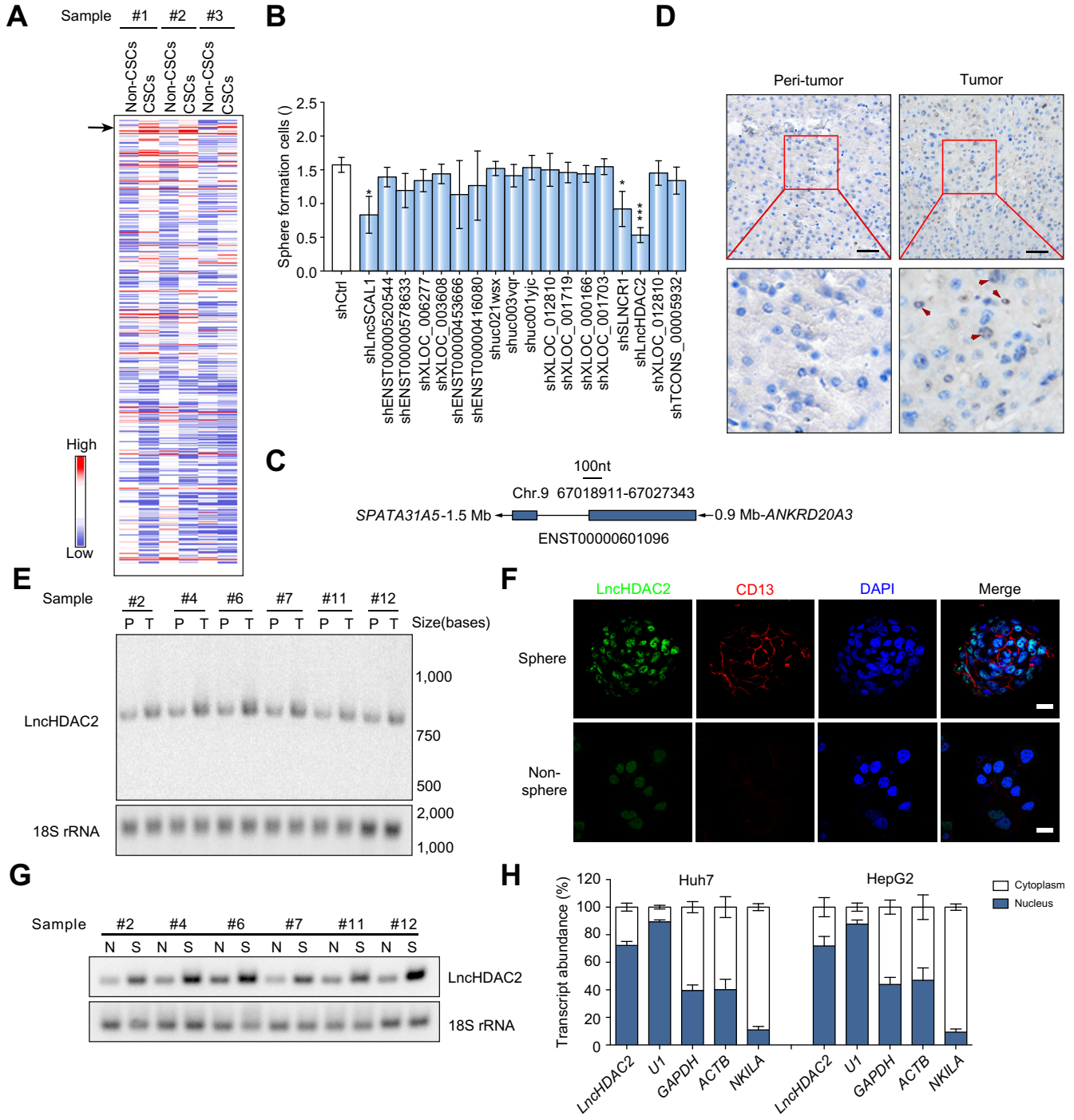

Fig. 1. *LncHDAC2* is highly expressed in liver CSCs. (A) Geometric mean-centered, hierarchical cluster heat map from microarray data. 665 annotated non-coding RNAs were represented in liver CSC ($CD13^{+}CD133^{+}$) compared with non- CSC ($CD13^{-}CD133^{-}$) cells sorted from HCC samples. Black arrowhead denotes *lncHDAC2*. (B) Top 20 upregulated lncRNAs in liver CSCs were depleted in HCC cells. Their sphere formation was tested via *in vitro* assays. Significance was calculated *vs.* shCtrl. Data are shown as means ± SD. $^{*}p$ <0.05 and $^{***}p$ <0.001 by 2-tailed Student's *t* test. Data are representative of at least 3 independent experiments. (C) Schematic annotation of *lncHDAC2* genomic locus on chromosome 9. Red rectangles denote exons. (D) Human HCC tumor and peri-tumor tissues were used for *lncHDAC2* hybridization. Six HCC samples showed similar results. Upper scale bars, 50 μm, lower scale bars, 20 μm. (E) Northern blots with *lncHDAC2* and 18S rRNA (loading control) probes. HCC samples were total RNA extracted from peri-tumor and tumor tissues. (F) Confocal micrographs of *lncHDAC2* and CD13, representing 3 independent experiments. DAPI, 4′,6-diamidino-2-phenylindole. Scale bars, 10 μm. (G) *LncHDAC2* and 18S rRNA (loading control) were examined by Northern blot. Total RNAs were extracted from spheres and non-spheres derived from HCC primary samples. (H) Cytoplasmic and nuclear fractionation of HCC oncosphere cell lysates followed by qRT-PCR detection. U1 RNA served as a positive control for nuclear location. Data are shown as means ± SD. (n = 3 cell cultures). CSCs, cancer stem cells; HCC, hepatocellular carcinoma; N, non-spheres; P, peri-tumor; qRT-PCR, quantitative reverse transcription PCR; S, spheres; T, tumor.

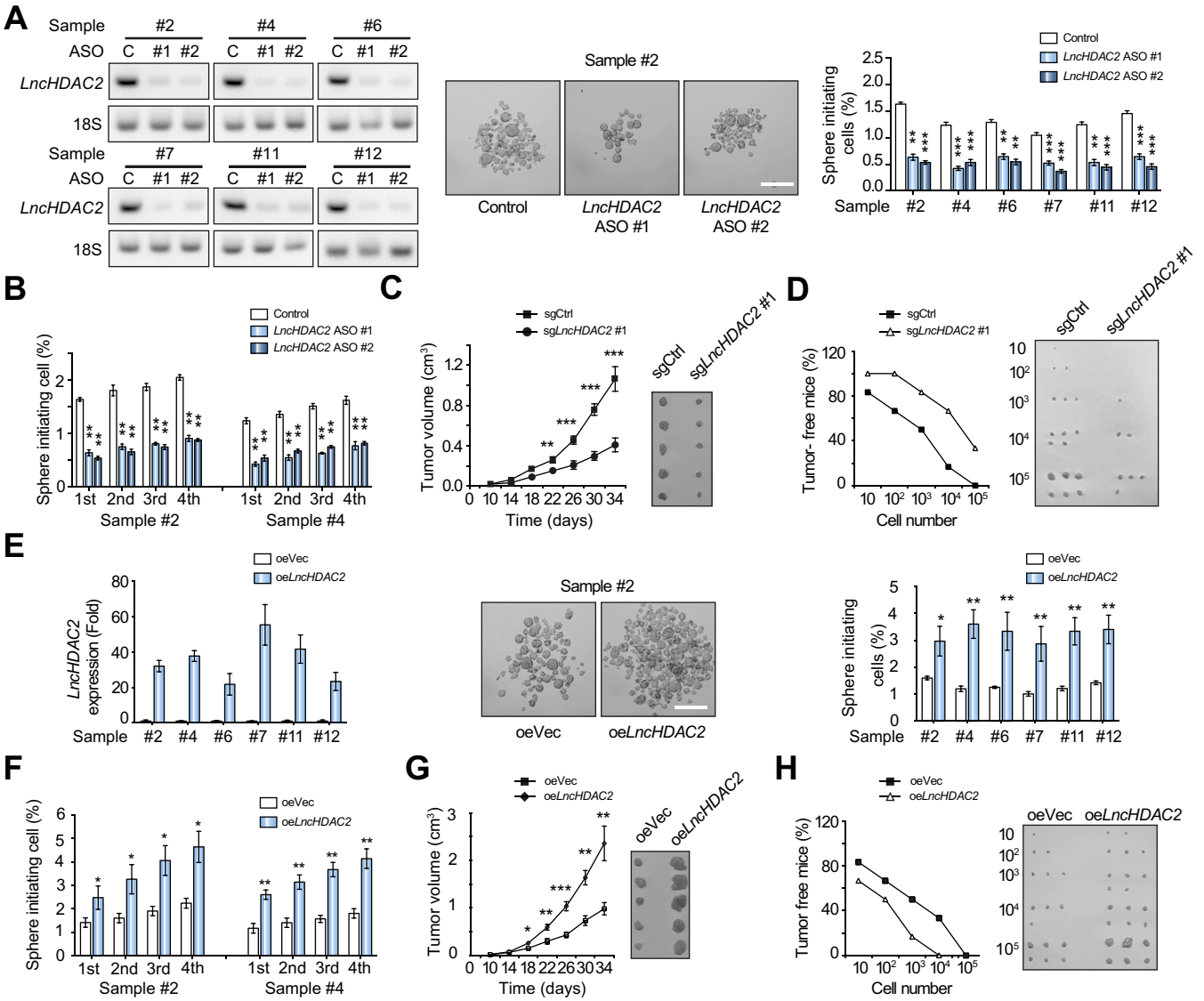

Fig. 2. *LncHDAC2* promotes the self-renewal maintenance of liver CSCs. (A) *LncHDAC2* silenced HCC primary tumor cells were established using ASOs and confirmed by Northern blot (left panels), followed by sphere-formation assays. Typical images (middle panels) and sphere-formation ratios (right panels) are shown. Scale bars, 500 μm. Data are shown as means ± SD. (n = 3 cell cultures) (B) Sphere-formation ratios of serial sphere formation. Six HCC primary tumor cells showed similar results. Error bars, SD (n = 3 cell cultures). (C) Tumor-volume curves of *lncHDAC2* knockout tumors. 1×10^6 *lncHDAC2* KO and control primary HCC cells were injected into BALB/c nude mice. Error bars, SD (n = 5 mice). Images of tumors are shown in right panel. (D) Ratios of tumor-free mice after 3 months' tumor formation after injection of increasing numbers of *lncHDAC2* KO and control cells. Images of tumors are shown in right panel. n = 6 mice for each group. (E) *LncHDAC2* expression, typical sphere images and plots of sphere-formation ratios of *lncHDAC2*–overexpressing (oe*LncHDAC2*) and empty vector control (oeVec) cells. Scale bars, 500 μm. Data are shown as means ± SD. (n = 3 cell cultures). (F) Sphere-formation ratios of serial sphere formation with overexpressing *lncHDAC2*. Six HCC primary tumor cells showed similar results. Data are shown as means ± SD. (n = 3 cell cultures). (G, H) Corresponding *in vivo* tumor propagation (G) and tumorigenic cell frequency (H) assays with overexpressing *lncHDAC2* (oe*LncHDAC2*). Throughout fig., $^{*}p$ <0.05; $^{**}p$ <0.01; $^{***}p$ <0.001 by 2-tailed Student's *t* test. ASOs, Antisense oligonucleotides; CSCs, cancer stem cells; HCC, hepatocellular carcinoma; KO, knockout.

not enrich on the *PTCH1* promoter region in *lncHDAC2* KO oncospheres (Fig. 4I). As a consequence, H4K5 and H3K9 acetylation levels were improved (Fig. 4J). Overexpression of *lncHDAC2* in *lncHDAC2* deleted cells could rescue the phenotypes, while overexpression of the mutant *lncHDAC2* failed (Fig. 4I, J). These data indicate that *lncHDAC2* recruits the NuRD complex onto the promoter of *PTCH1* gene to suppress its expression.

LncHDAC2-mediated PTCH1 downregulation promotes Hh signaling activation and drives the self-renewal of liver CSCs

PTCH1 is a twelve-pass transporter-like Hh receptor that prevents the 7-transmembrane protein Smo from coupling to Gli transcription factors.[32] We deleted HDAC2 and PTCH1 in HCC primary cells and HCC cell lines (Fig. S6A, B). We found that PTCH1 deletion augmented Smo activity, whereas *lncHDAC2* or HDAC2 deletion decreased the activity of Smo by GloSensor cAMP assay[33] (Fig. 5A). The absence of HDAC2 promotes proteasomal degradation of the Gli transcription factors GLI2 and GLI3, resulting in increased production of their corresponding repressor forms, GLI2R and GLI3R.[34,35] Of note, we showed that PTCH1 deletion decreased GliR levels, whereas *lncHDAC2* or HDAC2 deletion increased the GliR levels (Fig. 5B). In addition, we found that GLI2 was strongly stained in the nuclei of liver CSCs by immunohistochemical staining (Fig. S7A). Through RNA-FISH

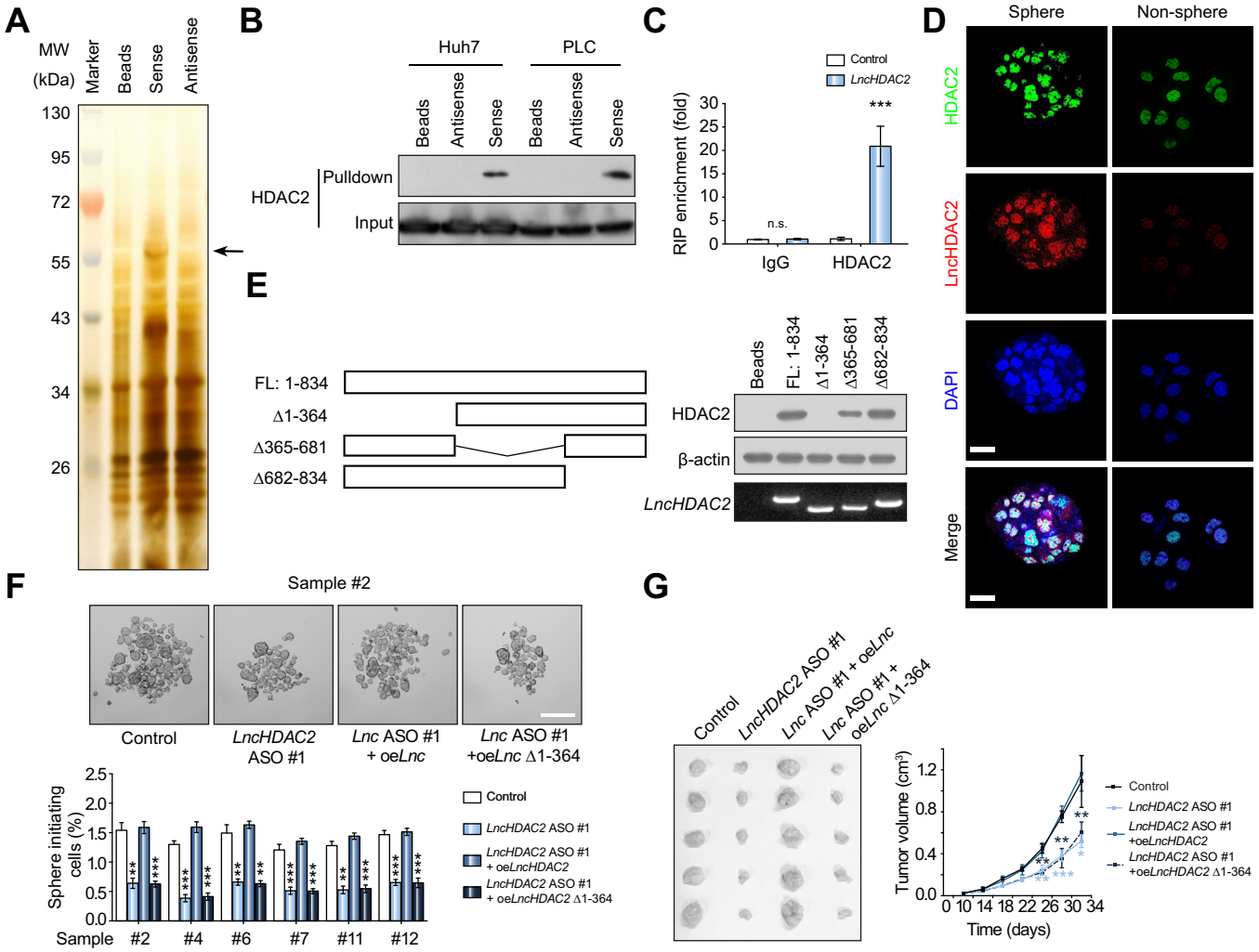

Fig. 3. *LncHDAC2* associates with HDAC2 in liver CSCs. (A) Digoxin RNA antisense purification (RAP) was performed using HCC primary oncosphere lysates, followed by mass spectrometry. Antisense, *lncHDAC2* reverse-complement transcript; sense, *lncHDAC2* transcript. A major differential band was identified to be HDAC2. (B) HCC samples were performed for RNA pulldown from oncospheres derived from HCC cell lines, followed by immunoblotting. (C) RNA immunoprecipitation (RIP) from HCC primary oncospheres with anti-HDAC2. Fold enrichment relative to IgG-precipitated ACTB was plotted. Data are shown as means ± SD. (n = 4 independent experiments). (D) Co-localization of *lncHDAC2* probes and anti-HDAC2 staining in oncospheres (top) and non-sphere cells (bottom). Scale bars, 10 μm. (E) Mapping analysis of HDAC2-binding domains of *lncHDAC2*. Schematic diagram of full-length and truncated fragments of *lncHDAC2* (top panel), western blot of HDAC2 in RNA pulldown samples by different *lncHDAC2* fragments (bottom panel). (F) Sphere formation was performed with *lncHDAC2*-depleted HCC primary cells and overexpressing *lncHDAC2* (oeLnc) or mutant *lncHDAC2* without HDAC2 binding domain (oeLncΔ1-364) in *lncHDAC2*-depleted cells. Scale bars, 500 μm. Six HCC samples obtained similar results. (G) Tumor-volume curves of 1×10^6 *lncHDAC2* knockdown cells, *lncHDAC2* knockdown cells overexpressing *lncHDAC2* (oeLnc) or mutant *lncHDAC2* without HDAC2 binding domain (oeLncΔ1-364), and control cells injected into BALB/c nude mice. Red *, for Control *vs. lncHDAC2* ASO #1; blue *, for *lncHDAC2* ASO #1 + oe*lncHDAC2 vs. lncHDAC2* ASO #1 + oe*lncHDAC2* Δ1-364. Data are shown as means ± SD. (n = 5 mice). Images of tumors are shown in left. Throughout fig., ns, no significance; *p <0.05; **p <0.01; ***p <0.001 by 2-tailed Student's t test. ASOs, antisense oligonucleotides; CSCs, cancer stem cells; HCC, hepatocellular carcinoma; MW, molecular weight.

assay, GLI2 was co-localized with *lncHDAC2* in oncosphere cells (Fig. S7B), suggesting that *lncHDAC2* activates Hh signaling. Consequently, PTCH1 deletion promoted downstream target genes of Hh signaling, while *lncHDAC2* or HDAC2 deletion suppressed these target genes (Fig. 5C). We next deleted the HDAC2-binding region of *PTCH1* promoter (*PTCH1* PKO) using a CRISPR/Cas9 approach. As expected, *PTCH1* PKO cells could promote oncosphere formation and tumor propagation capacity (Fig. 5D-F, Fig. S8A). In *PTCH1* PKO cells, *lncHDAC2* depletion has no effect on oncosphere formation and tumor propagation capacity (Fig. 5D-F, Fig. S8A), suggesting *lncHDAC2*-mediated promotion of liver CSC self-renewal is dependent on the PTCH1 expression. Since cyclopamine is a specific inhibitor against Smo, we then used cyclopamine to treat cells for oncosphere formation assays. We observed that cyclopamine treatment could impair *PTCH1* deletion-induced oncosphere formation and tumor propagation capacity (Fig. 5G-I), suggesting PTCH1-mediated Hh signaling is required for the self-renewal of liver CSCs. Collectively, *lncHDAC2*-mediated PTCH1 downregulation promotes Hh signaling activation and drives the self-renewal of liver CSCs and tumor propagation.

HDAC2 and PTCH1 expression levels are related to HCC severity

We analyzed the expression levels of HDAC2 using online available data sets. We noticed that HDAC2 was highly expressed in HCC tumors, especially in tumors with high rates of metastasis

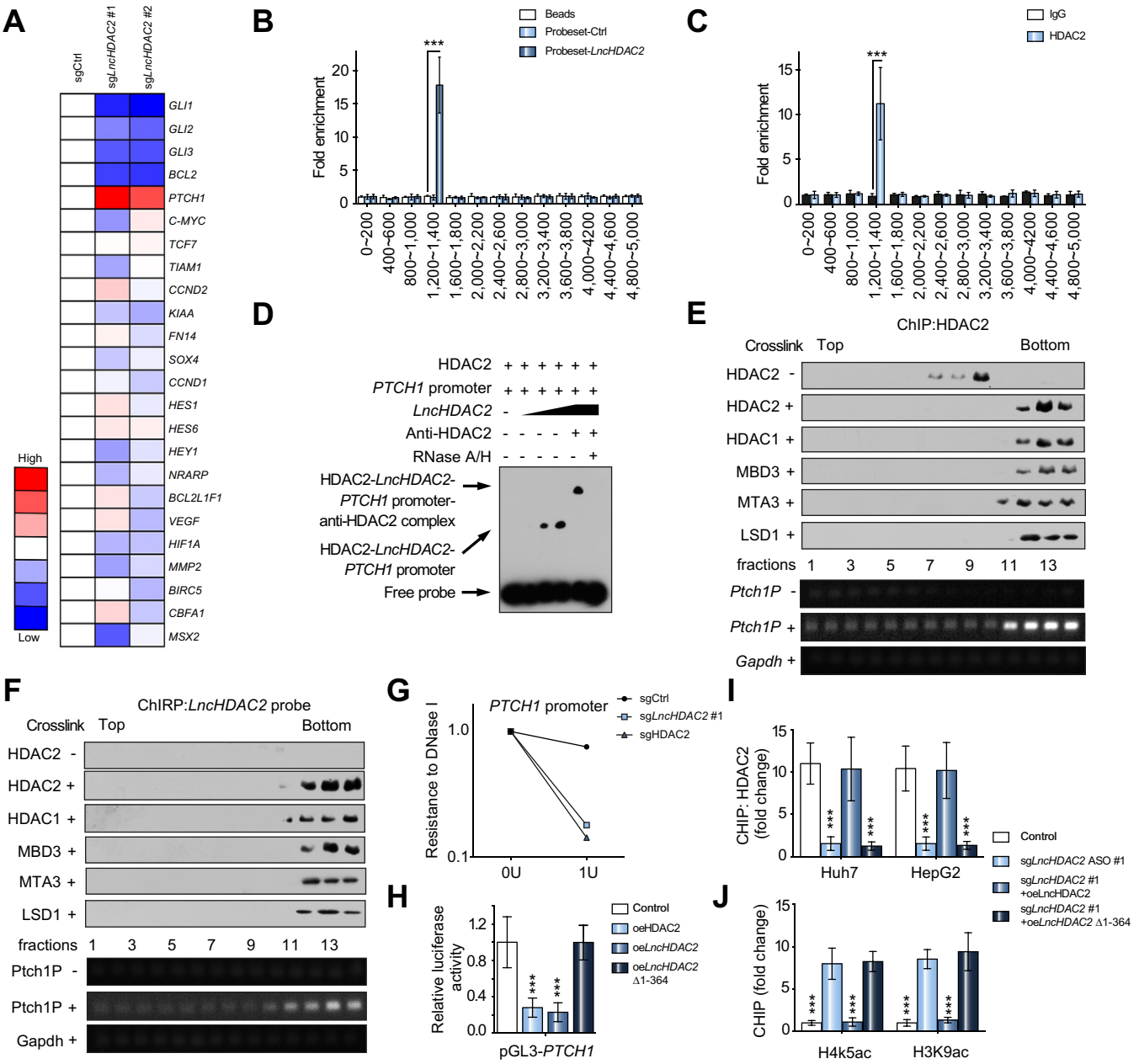

Fig. 4. HDAC2 and *lncHDAC2* enrich on *PTCH1* promoter to suppress its expression. (A) Indicated main stemness signaling pathways were analyzed in *lncHDAC2* KO spheres by qRT-PCR. (B) *PTCH1* promoter enrichment of *lncHDAC2* by ChIRP eluates. Probeset-Ctrl, Probeset-*lncHDAC2* were used for ChIRP assay, and enrichment of the indicated regions were examined by qPCR. (C) Huh7 cell lysates were performed for chromatin immunoprecipitation with HDAC2 or control (IgG) antibodies, followed by qPCR. IgG enrichment served as a control. (D) *PTCH1* promoter, HDAC2 protein, *lncHDAC2* transcript and anti-HDAC2 antibody were incubated for EMSA. *PTCH1* promoter was obtained by PCR and *lncHDAC2* was achieved using *in vitro* transcription. (E) ChIP eluates against HDAC2 were conducted for sucrose gradient ultracentrifugation, and elution fractions were analyzed by Western blot (upper panel) and PCR (lower panels). (F) ChIRP assay with Probeset-*lncHDAC2*. Eluents were subjected to sucrose gradient ultracentrifugation, followed by Western blot (upper panel) and PCR (lower panel). (G) *lncHDAC2* KO or HDAC2 KO increases chromatin accessibility at the promoter of *PTCH1* by DNase I digestion assays. (H) *PTCH1* promoter engagement by HDAC2 and *lncHDAC2* was validated by luciferase assay. *lncHDAC2* KO cells, *lncHDAC2* KO cells overexpressing *lncHDAC2* or mutant *lncHDAC2* without HDAC2 binding domain were used. (I) Indicated oncosphere lysates were prepared for chromatin immunoprecipitation with HDAC2 or control (IgG) antibodies, followed by examination of *PTCH1* promoter enrichment. (J) Indicated oncosphere lysates were prepared for chromatin immunoprecipitation with H4K5ac, H3K9ac or control (IgG) antibodies, followed by qPCR. IgG enrichment served as a control. Throughout fig., ***p <0.001 by 2-tailed Student's t test. ChIP, chromatin immunoprecipitation; CHIRP, chromatin isolation by RNA purification; CSCs, cancer stem cells; HCC, hepatocellular carcinoma; KO, knockout; qPCR, quantitative PCR; qRT-PCR, quantitative reverse transcription PCR.

(Fig. 6A). High expression levels of HDAC2 in HCC tumors also appeared in the TCGA dataset (Fig. S9A). In parallel, expression levels of HDAC2 were also positively related to HCC severity (Fig. 6B). These observations were further validated by examination of HCC samples with immunoblotting (Fig. 6D) and immunohistochemical staining (Fig. 6E). Moreover, HDAC2 was highly expressed in oncosphere cells by western blot (Fig. 6F) and immunofluorescence staining (Fig. 6G). As components of the NuRD complex, HDAC1 and CHD3 were also highly expressed in HCC and liver CSCs (Fig. 6D, F). High expression

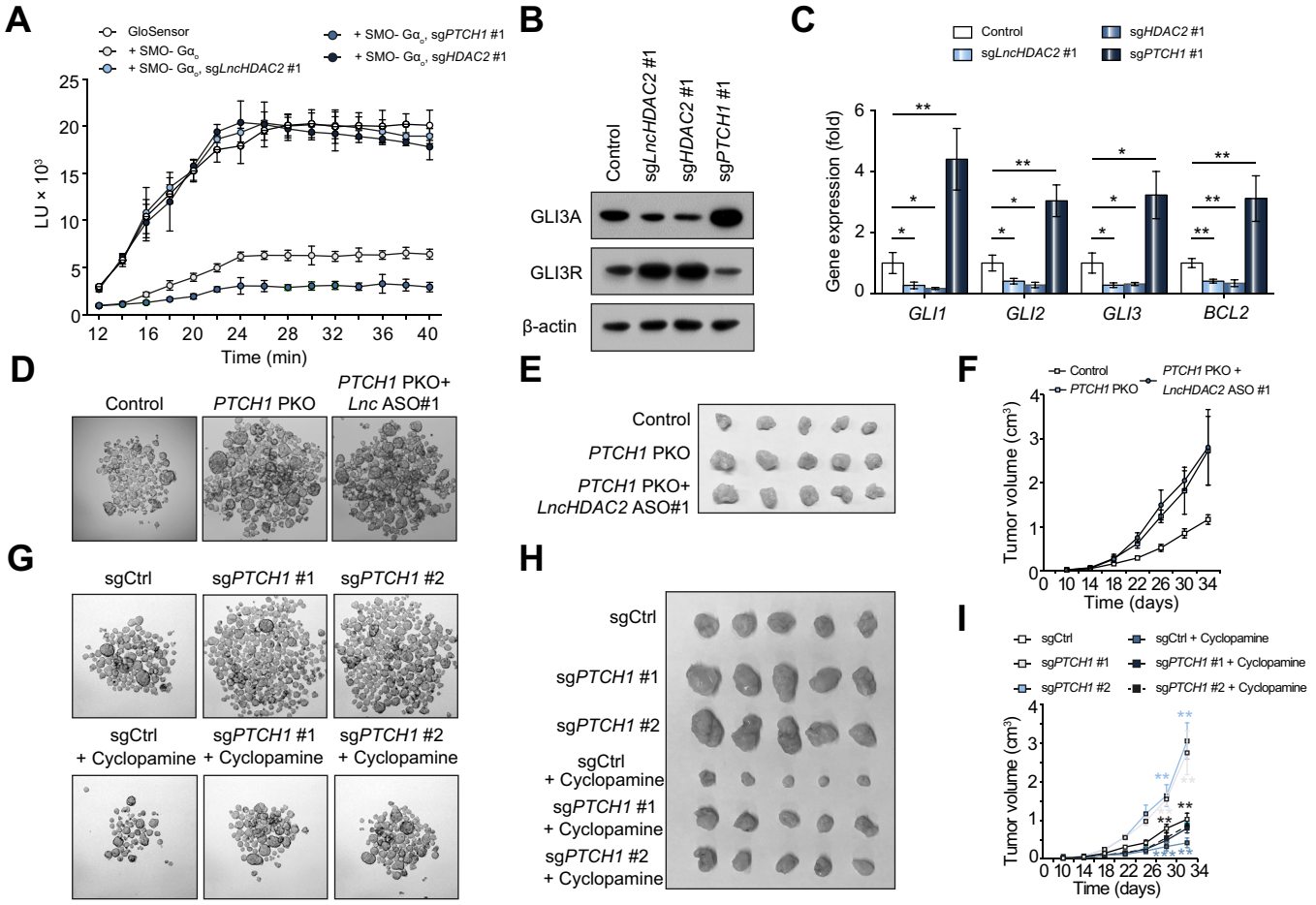

Fig. 5. PTCH1 suppresses self-renewal of liver CSCs via blocking Hedgehog signaling. (A) Live-cell luminescence traces from Huh7 cells transfected with indicated plasmids. Baseline luminescence was recorded for 10 min, followed by forskolin treatment and continued monitoring at 2 min intervals. (B) Whole-cell lysates of *lncHDAC2, HDAC2* or *PTCH1* KO cells were immunoprecipitated with anti-GLI3 antibody. GLI3A, full-length GLI3. GLI3R, repressor form of GLI3. (C) Hedgehog signaling target genes were examined in *lncHDAC2, HDAC2* or *PTCH1* KO cells by qRT-PCR. Data are shown as means ± SD. Data are representative of at least 3 independent experiments. (D) *PTCH1* promoter deletion in primary HCC cells (*PTCH1* PKO) and *lncHDAC2* depletion in *PTCH1* PKO cells (*PTCH*1 PKO + Lnc ASO #1) were performed for sphere formation. Representative sphere formation is shown. Scale bar, 500 μm. (E) 1×10^6 *PTCH1* PKO cells, *PTCH1* PKO cells depleting *lncHDAC2* and control cells were injected into BALB/c nude mice, and Images of tumors are shown. (F) Tumor-volume curves of 1×10^6 *PTCH1* PKO, *PTCH1* PKO + LncHDAC2 ASO #1 and control cells injected into BALB/c nude mice. Data are shown as means ± SD. (n = 5 mice). (G) Smo inhibitor cyclopamine blocks the increased self-renewal caused by PTCH1 KO. Representative sphere formation is shown. Scale bars, 500 μm. (n = 6 cell cultures). (H) 1×10^6 PTCH1 KO cells, PTCH1 KO cells with cyclopamine, control cells and control cells with cyclopamine were injected into BALB/c nude mice. Images of tumors are shown. (I) Tumor-volume curves of 1×10^6 PTCH1 KO cells, PTCH1 KO cells with cyclopamine, control cells and control cells with cyclopamine injected into BALB/c nude mice. Data are shown as means ± SD. (n = 5 mice). Red *, for sgCtrl *vs.* sgPTCH1 #1; green *, for sgCtrl *vs.* sgPTCH1 #2; pink *, for sgPTCH1 #1 *vs.* sgPTCH1 #1 + cyclopamine; turquoise *, for sgPTCH1 #2 *vs.* sgPTCH1 #2 + cyclopamine. Images of tumors are shown. Throughout fig., $^*p$ <0.05; $^{**}p$ <0.01; $^{***}p$ <0.001 by 2-tailed Student's *t* test. ASOs, antisense oligonucleotides; CSCs, cancer stem cells; KO, knockout; PKO, promoter KO; qRT-PCR, quantitative reverse transcription PCR.

levels of HDAC1 and CHD3 in HCC tumors also displayed in TCGA dataset (Fig. S9A). In addition, patients with HCC and higher expression of HDAC2 displayed worse prognosis in Wang's cohort (GSE14520) (Fig. 6C). Finally, HDAC2 deletion or suppression markedly suppressed *in vitro* oncosphere formation as well as *in vivo* tumor propagation (Fig. 6H, I, Fig. S9B, C). These data indicate that HDAC2 expression levels are positively related to HCC severity.

Based on analysis of Wang's cohort (GSE14520) and the TCGA dataset, we found that *PTCH1* was poorly expressed in patients with HCC (Fig. 6J, Fig. S9D). This observation was verified by examination of HCC samples and oncospheres with immunoblotting (Fig. 6K, M) and immunohistochemical staining (Fig. 6L), indicating that *PTCH1* expression levels are negatively related to HCC severity. Altogether, *HDAC2* and *PTCH1* expression levels are related to HCC severity.

Discussion

Nowadays, the CSC model has been verified in a variety of solid tumors.[4,36,37] These CSCs within tumor bulk display the capacity to self-renew, differentiate, and give rise to a new tumor.[38,39] We previously isolated a small subpopulation from HCC cell lines and HCC samples with 2 combined surface makers (CD13 and CD133) and defined this subset of $CD13^+CD133^+$ cells as liver CSCs.[8,40] In this study, we identified a lncRNA termed *lncHDAC2* that is highly expressed in HCC tumors and liver CSCs. *LncHDAC2* is required for the self-renewal of liver CSCs and tumor propagation. In liver CSCs, *lncHDAC2* interacts with HDAC2, which recruits the NuRD complex onto the promoter of *PTCH1* inhibiting its expression and leading to activation of Hh signaling. Moreover, HDAC2 expression levels are positively related to HCC severity and PTCH1 levels are negatively related to HCC severity.

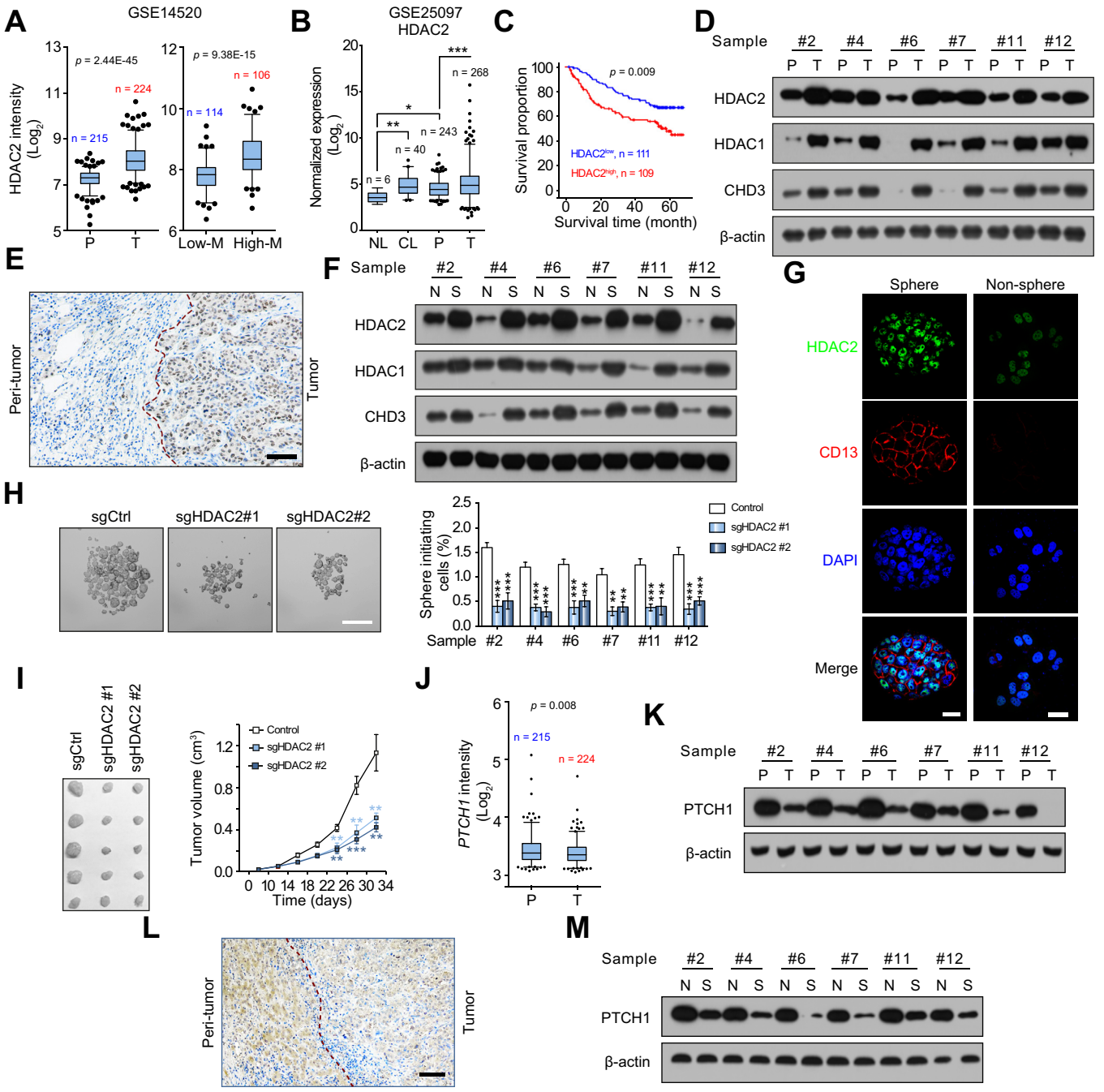

Fig. 6. HDAC2 and Hedgehog signaling activation are positively related to HCC severity. (A) Elevated *HDAC2* expression in HCC tumor tissues and high metastatic HCC patients derived from Wang's cohort (GSE14520). R language was used for gene expression analysis. (B) Elevated *HDAC2* expression in HCC tumor tissues derived from Zhang's cohort (GSE25097). R language was used for gene expression analysis. (C) Kaplan–Meier survival analysis of HCC samples from the mRNA cohort (GSE14520). Patients were divided into 2 groups on the basis of the indicated gene expression levels. (D, E) Immunoblotting against HDAC2, HDAC1 and CHD3 (D) and immunohistochemistry with anti-HDAC2 (E) were performed in HCC samples. β-actin served as a loading control. Scale bars, 100 μm. (F) Samples were immunoprecipitated from spheres and non-spheres derived from HCC primary cells, followed by western blotting. (G) Confocal images of HDAC2 and CD13 in oncospheres (top panel) and non-sphere cells (bottom panel). Scale bars, 10 μm. (H) Sphere-formation ability of HDAC2 KO cells from HCC primary samples. Typical micrograph images and plots of sphere-formation ratios are both shown. Scale bars, 500 μm. Data are shown as means ± SD. (n = 3 cell cultures). (I) Tumor-volume curves of 1×10^6 HDAC2 KO and control cells injected into BALB/c nude mice. Error bars, SD (n = 5 mice). Red *, for Control *vs.* sgHDAC2 #1; blue *, for Control *vs.* sgHDAC2 #2. Images of tumors are shown. (J) Low *PTCH1* expression in HCC tumor tissues from Wang's cohort (GSE14520). R language was used for gene expression analysis. (K) PTCH1 was tested in HCC primary samples by immunoblotting. (L) Immunohistochemistry with anti-PTCH1 was performed in HCC primary samples. Scale bars, 100 μm. (M) Samples were immunoprecipitated from spheres and non-spheres derived from HCC primary cells, followed by immunoblotting. For A, B, and J, data are shown as box-and-whisker plots. Whiskers below and above boxes extend to the 5th and 95th percentiles, respectively. Horizontal lines within boxes represent median levels of gene intensity. Boxes represent interquartile range (IQR); upper and lower edges correspond to the 75th and 25th percentiles, respectively. Throughout fig., *p <0.05; **p <0.01; ***p <0.001 by 2-tailed Student's t test. CL, cirrhosis liver; HCC, hepatocellular carcinoma; High-M, high rate of metastasis; KO, knockout; Low-M, low rate of metastasis; N, non-spheres; NL, normal liver; P, peri-tumor; S, spheres; T, tumor.

The non-coding RNA family includes more than 16 categories of long and short RNA molecules with different functional and structural characteristics.[41–43] Long non-coding RNAs (lncRNAs) are defined as transcripts longer than 200 nucleotides that are 5′ capped and 3′ polyadenylated, yet this class of transcripts has weak coding potential. Accumulating evidence shows that a bunch of lncRNAs are implicated in the regulation of tumorigenesis.[44] We previously identified several lncRNAs from liver CSCs of HCC cell lines and revealed their roles in the regulation of liver CSC stemness.[23–25] To further identify physiological lncRNAs involved in liver CSCs, we conducted transcriptome microarray analysis of liver CSCs and non-CSCs sorted from 3 HCC primary tumor tissues. Among the most upregulated lncRNAs, we identified *lncHDAC2* which promotes the self-renewal of liver CSCs by initiating Hh signaling pathway activation. Of note, *lncHDAC2* depletion by ASOs markedly reduced the self-renewal capacity of liver CSCs. We found that lnc-β-Catm was highly expressed in HCC sample #2 of the 3 HCC primary tumor tissues used for the transcriptome assay. Since there is great heterogeneity in HCC, some lncRNAs are only expressed in certain populations of patients with HCC. In addition, we observed that *lncHDAC2* knockdown did not affect the expression levels of *lncTCF7*, *lnc-β-Catm*, and *lncBrm*. Meanwhile, knockdown of *lncTCF7*, *lnc-β-Catm*, or *lncBrm* did not influence the expression level of *lncHDAC2* and did not impact Hh signaling in liver CSCs either. These data suggest that these lncRNAs have redundant functions in the regulation of liver CSC stemness. Here we showed that *lncHDAC2* bound to the 1,200–1,400 base pair region of the *PTCH1* promoter to regulate its transcription. Through analysis of their primary sequences, this binding of *lncHDAC2* to *the PTCH1* promoter did not rely on sequence complementary. Since *lncHDAC2* harbors several stem-loop structures, *lncHDAC2* may form tertiary topological structures that may mediate the binding of *lncHDAC2* to the *PTCH1* promoter. Another reason could be that *lncHDAC2*-interacting proteins mediate the binding of *lncHDAC2* to the *PTCH1* promoter. How *lncHDAC2* binds to *PTCH1* promoter needs to be investigated further.

The NuRD (also known as Mi-2) complex is a multisubunit chromatin remodeling complex.[45] It contains 2 core subunits, CHD3 and CHD4 ATP-dependent chromatin remodeling catalases, and HDAC1 with HDAC2 mediating histone or protein deacetylation.[46] The NuRD complex has been reported to play a critical role in transcriptional repression. Like other chromatin remodelers such as SWI/SNF and Polycomb complexes, the NuRD complex has been implicated in the transcriptional regulation involved in oncogenesis and cancer progression.[47,48] For instance, a truncated mutation of HDAC2 has been documented in sporadic carcinomas with microsatellite instability.[49] We previously showed that Sox2 recruits the NuRD complex to inhibit mTOR transcription, leading to cellular reprogramming.[46] Here we demonstrated that *lncHDAC2* interacts with HDAC2 that recruits the NuRD complex to repress PTCH1 expression. The suppression of PTCH1 expression promotes Smo activity, initiating Hh signaling, which is involved in the self-renewal of liver CSCs.

Hh signaling is essential for various processes during organ development and maintenance of organ functions.[50] The ability of the Hh pathway to modulate cell differentiation and renewal also means that deregulation of this pathway may result in uncontrolled cell fate.[51] Misregulation of Hh signaling has been reported to cause formation of basal-cell medulloblastoma and myeloid leukemia.[52] We previously showed that Hh signaling is required for the self-renewal of bladder cancer CSCs and that the Smo inhibitor cyclopamine abrogates bladder tumorigenesis.[16] Of note, we showed that *lncHDAC2*-mediated Hh signaling drives the stemness of liver CSCs and cyclopamine can impair the self-renewal of liver CSCs and suppress tumor propagation as well. Therefore, our findings suggest that downregulating *lncHDAC2* will provide a potent antitumor strategy against HCC.

Financial support

This work was supported by the National Natural Science Foundation of China (91640203, 31530093, 81330047, 31771638, 81672897, 81602247), Strategic Priority Research Programs of the Chinese Academy of Sciences (XDA12020219, XDB19030203), Beijing Natural Science Foundation (7181006, 7162125). Postdoctoral Innovative Talent Support Program to Pingping Zhu.

Conflict of interest

The authors declare no conflicts of interest that pertain to this work.

Please refer to the accompanying ICMJE disclosure forms for further details.

Authors' contributions

J.W. designed and performed experiments, analyzed data and wrote the paper; P.Z., T.L., Y.W., and Y.D. performed experiments and analyzed data; L.H., J.W., Y.H., J.L. performed some experiments; L.H provided HCC samples and analyzed data; B.Y., B. L., Y.G., L.Y. analyzed data. Z.F. initiated the study, organized, designed, and wrote the paper.

Accession number

Microarray data have been deposited in the NCBI GEO under accession number GSE122420.

Acknowledgement

We thank Drs. Yihui Xu and Yan Teng for technical support.

Supplementary data

Supplementary data to this article can be found online at https://doi.org/10.1016/j.jhep.2018.12.015.

References

[1] Torre LA, Bray F, Siegel RL, Ferlay J, Lortet-Tieulent J, Jemal A. Global cancer statistics, 2012. CA Cancer J Clin 2015;65:87–108.
[2] Ito K, Suda T. Metabolic requirements for the maintenance of self-renewing stem cells. Nat Rev Mol Cell Bio 2014;15:243–256.
[3] Bruix J, Gores GJ, Mazzaferro V. Hepatocellular carcinoma: clinical frontiers and perspectives. Gut 2014;63:844–855.
[4] Kreso A, Dick JE. Evolution of the cancer stem cell model. Cell Stem Cell 2014;14:275–291.
[5] Visvader JE, Lindeman GJ. Cancer stem cells in solid tumours: accumulating evidence and unresolved questions. Nat Rev Cancer 2008;8:755–768.
[6] Skvortsov S, Skvortsova II, Tang DG, Dubrovska A. Prostate cancer stem cells: current understanding. Stem Cells 2018.

[7] Yang ZF, Ho DW, Ng MN, Lau CK, Yu WC, Ngai P, et al. Significance of CD90+ cancer stem cells in human liver cancer. Cancer Cell 2008;13:153–166.
[8] Haraguchi N, Ishii H, Mimori K, Tanaka F, Ohkuma M, Kim HM, et al. CD13 is a therapeutic target in human liver cancer stem cells. J Clin Invest 2010;120:3326–3339.
[9] Kaur G, Sharma P, Dogra N, Singh S. Eradicating cancer stem cells: concepts, issues, and challenges. Curr Treat Options Oncol 2018;19:20.
[10] Takebe N, Miele L, Harris PJ, Jeong W, Bando H, Kahn M, et al. Targeting Notch, Hedgehog, and Wnt pathways in cancer stem cells: clinical update. Nat Rev Clin Oncol 2015;12:445–464.
[11] Matsui WH. Cancer stem cell signaling pathways. Medicine (Baltimore) 2016;95:S8–S19.
[12] Pasca di Magliano M, Hebrok M. Hedgehog signalling in cancer formation and maintenance. Nat Rev Cancer 2003;3:903–911.
[13] Ruiz i Altaba A, Sanchez P, Dahmane N. Gli and hedgehog in cancer: tumours, embryos and stem cells. Nat Rev Cancer 2002;2:361–372.
[14] Sharma N, Nanta R, Sharma J, Gunewardena S, Singh KP, Shankar S, et al. PI3K/AKT/mTOR and sonic hedgehog pathways cooperate together to inhibit human pancreatic cancer stem cell characteristics and tumor growth. Oncotarget 2015;6:32039–32060.
[15] Hebrok M, Kim SK, St Jacques B, McMahon AP, Melton DA. Regulation of pancreas development by hedgehog signaling. Development 2000;127:4905–4913.
[16] Luo S, Lu JY, Liu L, Yin Y, Chen C, Han X, et al. Divergent lncRNAs regulate gene expression and lineage differentiation in pluripotent cells. Cell Stem Cell 2016;18:637–652.
[17] Athar M, Li C, Kim AL, Spiegelman VS, Bickers DR. Sonic hedgehog signaling in Basal cell nevus syndrome. Cancer Res 2014;74:4967–4975.
[18] Hahne JC, Valeri N. Non-coding RNAs and resistance to anticancer drugs in gastrointestinal tumors. Front Oncol 2018;8:226.
[19] Anastasiadou E, Jacob LS, Slack FJ. Non-coding RNA networks in cancer. Nat Rev Cancer 2018;18:5–18.
[20] Ye B, Liu B, Yang L, Zhu X, Zhang D, Wu W, et al. LncKdm2b controls self-renewal of embryonic stem cells via activating expression of transcription factor Zbtb3. EMBO J 2018;37.
[21] Guo CJ, Zhang W, Gershwin ME. Long noncoding RNA lncKdm2b: a critical player in the maintenance of group 3 innate lymphoid cells. Cell Mol Immunol 2018;15:5–7.
[22] Liu B, Ye B, Yang L, Zhu X, Huang G, Zhu P, et al. Long noncoding RNA lncKdm2b is required for ILC3 maintenance by initiation of Zfp292 expression. Nat Immunol 2017;18:499–508.
[23] Zhu P, Wang Y, Huang G, Ye B, Liu B, Wu J, et al. lnc-beta-Catm elicits EZH2-dependent beta-catenin stabilization and sustains liver CSC self-renewal. Nat Struct Mol Biol 2016;23:631–639.
[24] Wang Y, He L, Du Y, Zhu P, Huang G, Luo J, et al. The long noncoding RNA lncTCF7 promotes self-renewal of human liver cancer stem cells through activation of Wnt signaling. Cell Stem Cell 2015;16:413–425.
[25] Zhu P, Wang Y, Wu J, Huang G, Liu B, Ye B, et al. LncBRM initiates YAP1 signalling activation to drive self-renewal of liver cancer stem cells. Nat Commun 2016;7:13608.
[26] Batista PJ, Chang HY. Long noncoding RNAs: cellular address codes in development and disease. Cell 2013;152:1298–1307.
[27] Beck B, Blanpain C. Unravelling cancer stem cell potential. Nat Rev Cancer 2013;13:727–738.
[28] Cech TR, Steitz JA. The noncoding RNA revolution-trashing old rules to forge new ones. Cell 2014;157:77–94.
[29] Engreitz J, Lander ES, Guttman M. RNA antisense purification (RAP) for mapping RNA interactions with chromatin. Methods Mol Biol 2015;1262:183–197.
[30] Dege C, Hagman J. Mi-2/NuRD chromatin remodeling complexes regulate B and T-lymphocyte development and function. Immunol Rev 2014;261:126–140.
[31] Lai AY, Wade PA. Cancer biology and NuRD: a multifaceted chromatin remodelling complex. Nat Rev Cancer 2011;11:588–596.
[32] Qi X, Schmiege P, Coutavas E, Wang J, Li X. Structures of human Patched and its complex with native palmitoylated sonic hedgehog. Nature 2018;560:128–132.
[33] Myers BR, Neahring L, Zhang Y, Roberts KJ, Beachy PA. Rapid, direct activity assays for smoothened reveal Hedgehog pathway regulation by membrane cholesterol and extracellular sodium. PNAS 2017;114:E11141–E11150.
[34] Haycraft CJ, Banizs B, Aydin-Son Y, Zhang Q, Michaud EJ, Yoder BK. Gli2 and Gli3 localize to cilia and require the intraflagellar transport protein polaris for processing and function. PLoS Genet 2005;1 e53.
[35] Wang B, Fallon JF, Beachy PA. Hedgehog-regulated processing of Gli3 produces an anterior/posterior repressor gradient in the developing vertebrate limb. Cell 2000;100:423–434.
[36] Al-Hajj M, Wicha MS, Benito-Hernandez A, Morrison SJ, Clarke MF. Prospective identification of tumorigenic breast cancer cells. Proc Natl Acad Sci U S A 2003;100:3983–3988.
[37] Nio K, Yamashita T, Kaneko S. The evolving concept of liver cancer stem cells. Mol Cancer 2017;16:4.
[38] Clevers H. The cancer stem cell: premises, promises and challenges. Nat Med 2011;17:313–319.
[39] Hermann PC, Huber SL, Herrler T, Aicher A, Ellwart JW, Guba M, et al. Distinct populations of cancer stem cells determine tumor growth and metastatic activity in human pancreatic cancer. Cell Stem Cell 2007;1:313–323.
[40] Ma S, Chan KW, Hu L, Lee TK, Wo JY, Ng IO, et al. Identification and characterization of tumorigenic liver cancer stem/progenitor cells. Gastroenterology 2007;132:2542–2556.
[41] Eddy SR. Non-coding RNA genes and the modern RNA world. Nat Rev Genet 2001;2:919–929.
[42] Li Z, Huang C, Bao C, Chen L, Lin M, Wang X, et al. Exon-intron circular RNAs regulate transcription in the nucleus. Nat Struct Mol Biol 2015;22:256–264.
[43] Gupta RA, Shah N, Wang KC, Kim J, Horlings HM, Wong DJ, et al. Long non-coding RNA HOTAIR reprograms chromatin state to promote cancer metastasis. Nature 2010;464:1071–1076.
[44] Yan X, Zhang D, Wu W, Wu S, Qian J, Hao Y, et al. Mesenchymal stem cells promote hepatocarcinogenesis via lncRNA-MUF interaction with ANXA2 and miR-34a. Cancer Res 2017;77:6704–6716.
[45] Clapier CR, Cairns BR. The biology of chromatin remodeling complexes. Annu Rev Biochem 2009;78:273–304.
[46] Wang S, Xia P, Ye B, Huang G, Liu J, Fan Z. Transient activation of autophagy via Sox2-mediated suppression of mTOR is an important early step in reprogramming to pluripotency. Cell Stem Cell 2013;13:617–625.
[47] Denslow SA, Wade PA. The human Mi-2/NuRD complex and gene regulation. Oncogene 2007;26:5433–5438.
[48] Wang Y, Zhang H, Chen Y, Sun Y, Yang F, Yu W, et al. LSD1 is a subunit of the NuRD complex and targets the metastasis programs in breast cancer. Cell 2009;138:660–672.
[49] Bantscheff M, Hopf C, Savitski MM, Dittmann A, Grandi P, Michon AM, et al. Chemoproteomics profiling of HDAC inhibitors reveals selective targeting of HDAC complexes. Nat Biotechnol 2011;29:255–265.
[50] Scales SJ, de Sauvage FJ. Mechanisms of Hedgehog pathway activation in cancer and implications for therapy. Trends Pharmacol Sci 2009;30:303–312.
[51] Clement V, Sanchez P, de Tribolet N, Radovanovic I, Ruiz i Altaba A. HEDGEHOG-GLI1 signaling regulates human glioma growth, cancer stem cell self-renewal, and tumorigenicity. Curr Biol 2007;17:165–172.
[52] Zhao C, Chen A, Jamieson CH, Fereshteh M, Abrahamsson A, Blum J, et al. Hedgehog signalling is essential for maintenance of cancer stem cells in myeloid leukaemia. Nature 2009;458:776–779.